PHYSICAL REVIEW B **77**, 020402(R) (2008)

Magnetotransport properties of mesoscopic graphite spin valves

W. H. Wang, K. Pi, Y. Li, Y. F. Chiang, P. Wei, J. Shi, and R. K. Kawakami*

Department of Physics and Astronomy, University of California, Riverside, California 92521, USA

(Received 6 May 2007; revised manuscript received 3 September 2007; published 8 January 2008)

We report the magnetoresistance (MR) properties of quasi-two-dimensional mesoscopic graphite (MG) spin valve devices consisting of MG flakes contacted by ferromagnetic (FM) electrodes. For devices in which an ultrathin magnesium oxide (MgO) tunnel barrier is inserted at the FM/MG interface, the spin valve effect has been observed, with MR magnitudes up to 12% at 7 K and signals persisting up to temperatures as high as 60 K. In contrast, the spin valve effect has not been seen in devices without MgO, suggesting the importance of spin-dependent interfacial resistance for spin injection into MG. In addition, an investigation of the voltage bias dependence and gate voltage dependence of MR has been performed.

DOI: 10.1103/PhysRevB.77.020402 PACS number(s): 75.47.−m, 72.25.−b, 72.25.Hg, 85.75.−d

Carbon-based nanostructures are attractive for spin-polarized electronics[1,2] because the low spin-orbit coupling (due to low atomic number) should lead to long spin coherence times. Among various forms of carbon-based nanostructures, carbon nanotubes (CNTs) are extensively used for studies of spin-dependent phenomenon. There has been significant progress including demonstrations of spin injection and transport,[3] enhancement of spin injection,[4] and electric field control of spin transport[5] in CNTs. Recently, due to the experimental realization of single-layer graphene,[6–8] there has been extensive theoretical interest in the spin-dependent properties of graphene including predictions of half-metallic graphene ribbons,[9] magnetic ordering in graphene,[10] and spin Hall effects.[11,12] Experimentally, there has been some evidence for spin-polarized transport in graphene spin valves,[13] but few studies have been reported. In this paper, we investigate the magnetoresistance (MR) properties of quasi-two-dimensional mesoscopic graphite (MG) spin valve devices consisting of MG flakes with thickness between 1 and 40 nm ($\sim$3 to $\sim$100 layers of graphene) contacted by two ferromagnetic (FM) electrodes. We observe signatures of spin-polarized transport for MG flakes in the thickness range 10–40 nm. For devices in which an ultrathin magnesium oxide (MgO) tunnel barrier is inserted at the FM/MG interface, the spin valve effect has been observed with MR magnitudes up to 12% at 7 K and signals persisting up to temperatures as high as 60 K. In contrast, the spin valve effect has not been seen in devices without MgO, suggesting the importance of spin-dependent interfacial resistance for spin injection into MG.[14,15] Investigation of the voltage bias dependence of the MR finds a reduction of the MR with increasing voltage and a correlation with the differential conductance. Finally, the spin valve signal exhibits oscillatory MR as a function of gate voltage.[5,16,17]

Fabrication of MG spin valves begins with the extraction of MG flakes from single-crystalline Kish graphite via sonication in a dichlorobenzene solution.[18] The MG is then dispersed and dried onto $SiO_2/Si(100)$ substrates with prepatterned gold electrodes and alignment marks. The MG flakes are regularly characterized by atomic force microscopy (AFM), scanning electron microscopy (SEM), and optical microscopy, and the locations of the most promising flakes are recorded. Electron beam lithography (EBL) is utilized to define the FM contacts to the MG. Figure 1(a) shows a SEM image of a typical device. The desired device geometry is to have rectangular FM contacts on the MG [vertical bars in Fig. 1(a)] and nonmagnetic (NM) wires [horizontal bars in Fig. 1(a)] extending away from the FM and connecting to prepatterned gold electrodes. Both the FM and NM regions can be defined from a single resist pattern by using angle evaporation, which is discussed in more detail below. In order to obtain the undercut pattern for the angle evaporation, we spin-coat a bilayer of electron beam resist (poly(methyl methacrylate)/methyl methacrylate) onto the $MG/SiO_2/Si(100)$, expose, and develop the desired EBL pattern.

MgO and metal evaporation through the patterned electron beam resist is performed in an ultrahigh-vacuum chamber with a base pressure of 2×10^{-10} torr. Metals are deposited from Knudsen cells or electron beam evaporators. Large-area FM films grown in this chamber consistently exhibit square hysteresis loops, indicating high material quality. The angle evaporation is based on a single rotation axis for the sample [dashed line in Fig. 1(a)] that is perpendicular to the evaporator plane. Rotating the sample can achieve normal incidence ($\theta=0°$) or non-normal incidence from two directions ($\theta>0°$ or $\theta<0°$). The sample is mounted with a fixed in-plane angle ($\phi\sim20°$) between the long axes of the FM electrodes and the evaporator plane so that changing the polar angle (θ) will induce shifts of the pattern in both the x and y directions. First, MgO is deposited onto the MG at two opposite angles away from normal (e.g., $\theta=+60°$ and $-60°$) to have the maximal coverage area on the MG. MgO films are formed by sequentially depositing a few angstroms of Mg and oxidizing with O_2 gas (>1000 langmuirs), and repeating until the final thickness is achieved. The typical MgO thickness is 1 nm for each layer, and the double angle evaporation generates a center region of the electrode with double MgO thickness. Following the MgO deposition, two different FM materials are deposited at angles somewhat closer to normal incidence, leading to a smaller coverage area than the MgO (to prevent direct contact between the FM and MG). Co (7 nm) and Fe (7 nm) are deposited from opposite directions so that the final device cross section is as given schematically in Fig. 1(c). The Fe and Co should be ferromagnetically coupled and there should be little variation of the

 ©2008 The American Physical Society

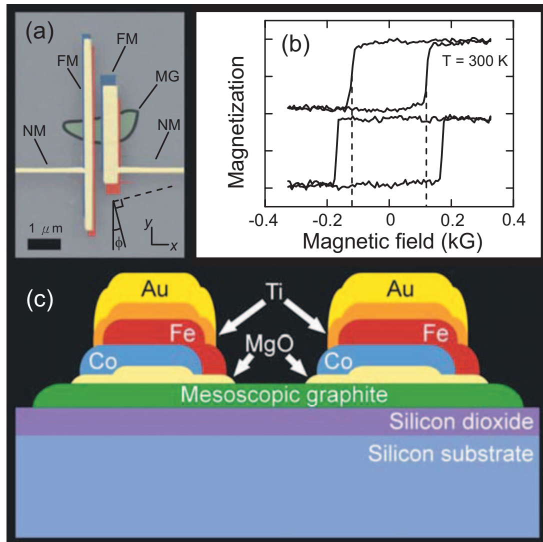

FIG. 1. (Color) (a) SEM image showing a typical device structure (colorized for clarity). Most of the electrode area is covered by gold (yellow), while part of the FM layers (red, blue) can be seen at the edges. The mesoscopic graphite (green) is barely visible and is outlined for clarity. (b) Room temperature magnetic hysteresis loops of test electrodes obtained by magneto-optic Kerr microscopy. The structures are identical to those shown in the SEM image but without the top Au layer. The top curve is for a 0.5×4 μm^2 electrode. The bottom curve is for a 0.2×8 μm^2 electrode. (c) A schematic of the cross section of a spin valve device with MgO tunnel barrier.

magnetization along the growth axis due to the low film thickness. Due to the two different MgO thickness regions, the current is likely to be dominated by tunneling across the thinner MgO and the spin injection should reflect the density of states of both Fe and Co, possibly in a complicated manner. The different shapes of the two FM electrodes separate their magnetization switching fields due to magnetic shape anisotropy. In this way, it is possible to achieve both parallel and antiparallel magnetization alignments of the FM electrodes as an external magnetic field is ramped. Finally, at normal incidence a thin Ti adhesion layer (4 nm) and gold layer (20 nm) are deposited to form the NM wires that connect the FM contacts to the prepatterned gold electrodes (which connect to external wires). Note that, due to the angle evaporation, neither the MgO nor the FM is deposited in the NM wire regions. Room temperature magnetic hysteresis loops of test electrodes with identical structure to those shown in Fig. 1(a) (but without the top Au layer) are obtained by magneto-optic Kerr microscopy [Fig. 1(b)]. The loops clearly show a single magnetization reversal, indicating that the Fe and Co layers are strongly ferromagnetically coupled, and different coercive fields are obtained for the different electrode shapes.

Samples are cooled in a liquid helium cryostat where magnetotransport measurements are performed. An external magnetic field is applied parallel to the sample surface and along the long axes of the FM electrodes. Transport measurements are performed in a two-point geometry by applying a finite bias and measuring the current. The two-terminal re-

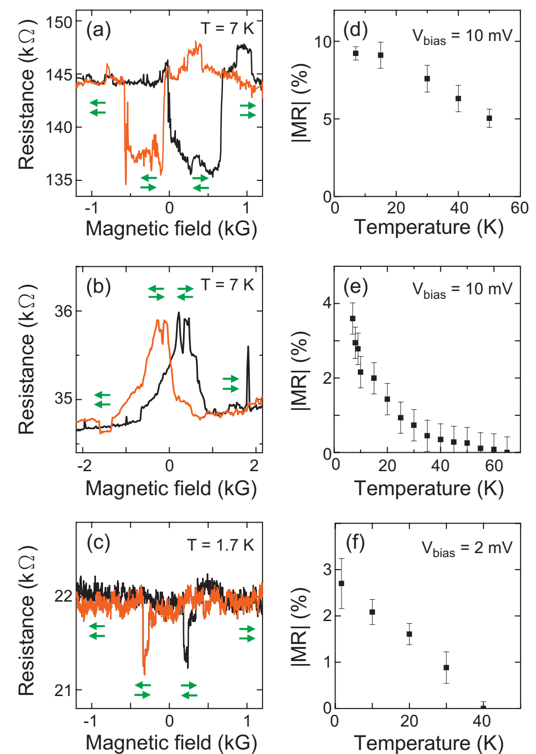

FIG. 2. (Color) (a)–(c) Two-terminal resistances measured during the magnetic field scan for samples A, B, and C, respectively. The thicknesses of MG in samples A, B, and C are 40, 30, and 10 nm, respectively. Black (red) curve corresponds to upward (downward) sweeping of the magnetic field. (d)–(f) Temperature dependences of magnetoresistance for samples A, B, and C, respectively.

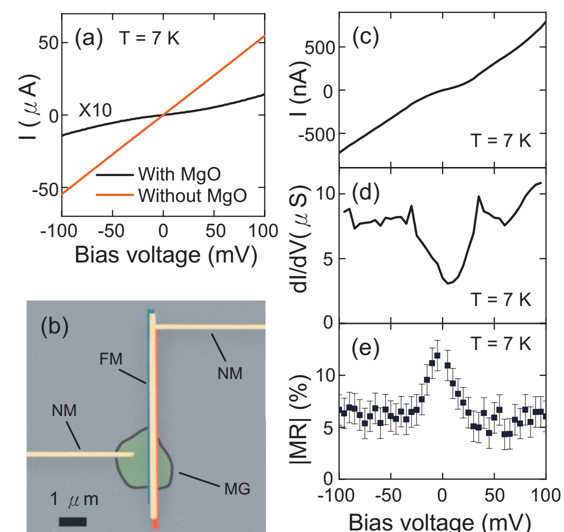

FIG. 3. (Color) (a) Comparison of I-V characteristics of devices with MgO (sample B) and without MgO tunnel barriers (sample D). (b) SEM image of a control sample with NM/MG/MgO/FM structure. The MG is colored green and outlined for clarity. (c) I-V curve for sample A. (d) Differential conductance of sample A obtained by numerical differentiation. (e) MR of sample A as a function of bias voltage.

sistances are dominated by junction resistance because the metallic lead resistances are less than 200 Ω. This is determined by measuring the resistance of a test sample in which the electrode structure in Fig. 1(c) is shorted by a patterned gold wire. The Si substrate is used as a back gate and unless otherwise stated, the gate voltage is zero.

Figures 2(a)–2(c) show the magnetic field dependences of resistance for three MG spin valve devices *A*, *B*, and *C*. The thicknesses of MG in samples *A*, *B*, and *C* are 40, 30, and 10 nm, respectively, where the thicknesses are determined by AFM after all magnetotransport measurements have been performed. These three samples have electrode gaps of 200 nm and have room temperature resistances of 45, 17, and 11 kΩ, respectively. As the magnetic field is ramped up or down, we observe two transitions in the device resistance corresponding to the two distinct coercivities of the FM electrodes. This magnetoresistance is attributed to the spin valve effect in which the resistance depends on the relative magnetization alignment of the two FM electrodes due to spin-polarized transport across the MG. For samples *A* and *C*, the MR is negative—the device resistance is lower for the antiparallel magnetization state of the FM electrodes. However, we observe positive MR for sample *B*, where device resistance is higher when FM electrodes are in an antiparallel magnetization state. Considering that the bulk Fermi level spin polarizations for Co and Fe (35% and 40%, respectively) have the same sign,[19] one would expect from a Julliere-type of analysis[20] that the MR should always be positive. However, in the case of a double-barrier structure with spin-preserving conduction channel,[16] both positive and negative MR are possible due to quantum interferences in the channel. In addition, it is possible that oxidized Co or Fe at the FM/MgO interface can change the sign of MR by changing the Fermi level spin polarization.[21] While the exact cause of the different MR signs is not yet clear, this behavior is consistent with the related CNT spin valves where the MR can be positive,[3] negative,[22] or controlled by gate voltage.[5,17,23] We note that there are small resistance jumps in the MR scans which do not repeat on subsequent scans. Surface antiferromagnetic oxides are likely to form at the edges of the FM electrodes where there is no gold cap. This could generate domain wall pinning sites to produce a gradual switching (as seen in sample *B*). Surface antiferromagnetic oxides may also generate asymmetric switching (as seen in sample *A*) through the exchange bias effect. Random inhomogeneities in the MgO barrier could generate a spatially varying tunneling rate, which would make the MR signals more sensitive to particular FM regions and could produce sample-to-sample variations in device resistance. To improve the MR characteristics and reduce sample-to-sample variations, optimization of the MgO barrier and the FM capping procedures are needed.

The temperature dependence of MR for samples *A*, *B*, and *C* are shown in Figs. 2(d)–2(f). Sample *A*, which exhibits the largest value of MR among our sample set, exhibits MR up to at least 50 K, but unfortunately the temperature dependence was not completed due to sample failure. The MR of sample *A* is 9% at 7 K and gradually decreases at a roughly uniform rate as temperature increases. The MR of sample *B* is 3.6% at 7 K and decreases in a nonlinear manner as temperature rises and disappears at 65 K. The MR for sample *C* is 2.7% at 1.7 K and decreases almost linearly as temperature increases, eventually disappearing at 40 K.

We have examined the role of MgO tunnel barriers by fabricating control samples with FM/MG/FM structure. No MR has been observed in any of these control samples. The current-voltage (*I-V*) characteristics of these devices are linear and device resistances are less than 2 kΩ at 2 K. For comparison, the devices with FM/MgO/MG/MgO/FM structure exhibit nonlinear *I-V* and have resistance 1–2 orders of magnitude higher. In Fig. 3(a), we show a comparison of two typical *I-V* characteristics of devices with MgO (sample *B*) and without MgO tunnel barrier (sample *D*). In our study, out of seven devices with nonlinear *I-V*, four have exhibited the spin valve signals. There have been significant discussions about the use of tunnel barriers for spin injection into semiconductors. Due to a conductivity mismatch between the metal FM and the semiconductor, the spin injection efficiency is greatly suppressed.[24] The insertion of a tunnel barrier between the FM and the semiconductor alleviates this problem,[14,15] and experiments using MgO tunnel barriers exhibit the highest spin injection efficiency into GaAs.[25] In our case, graphite is semimetallic with low-temperature (10 K) resistivity ranging from 3.0×10^{-8} to $1.0\times10^{-7}\ \Omega\,\mathrm{m}$,[26] roughly a few orders of magnitude larger than Fe and Co ($\rho_{\mathrm{Fe}}=1.0\times10^{-11}\ \Omega\,\mathrm{m}$, $\rho_{\mathrm{Co}}=1.0\times10^{-11}\ \Omega\,\mathrm{m}$).[27] Thus, tunnel barriers should improve the spin injection into MG.

It is arguable that the observed spin valve signals are not due to spin-polarized transport through MG, but to other effects such as anisotropic magnetoresistance. This type of magnetoresistance, however, should show in devices even with a single FM electrode contact. In order to exclude the possibility that the observed spin valve effect is due to those artifacts, we have fabricated control samples with the MG contacted by FM materials on one end and NM material on the other end. Figure 3(b) shows a SEM image of a typical device with such structures (NM/MG/MgO/FM). The device pattern is designed such that one end is relatively narrow (labeled as the NM region on the left), which leads to a purely NM contact due to the angle evaporation. The other contact consists of MgO/FM materials deposited on the vertical bars and is subsequently capped with NM material. For all control devices with these structures, we have not observed a spin valve signal under the same experimental conditions. This provides further evidence that the observed MR results from spin-polarized transport through the MG.

Figures 3(c) and 3(d) show the *I-V* curve for sample *A* and the differential conductance obtained by numerical differentiation. The differential conductance exhibits a strong dip near zero bias, and there is a slight asymmetry in the *I-V* characteristics. In Fig. 3(e), we show the bias dependence of MR, which varies from 6% to 12% depending on the bias voltage. When the bias voltage is less than 25 mV, the MR is significantly enhanced. We note that the bias dependence of MR is highly correlated with the device conductance. Although the cusplike feature of bias dependence of MR and correlation between device resistance and MR have been seen in magnetic tunnel junctions,[28] it was not as pronounced as in our device. We also note that for all samples measured,

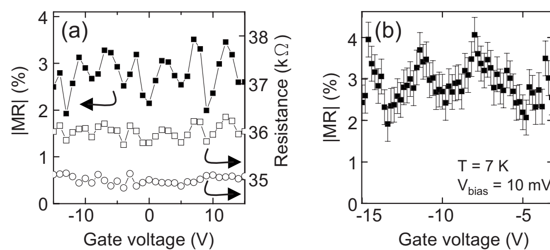

FIG. 4. (a) Gate voltage dependence of the MR (solid squares), R_{AP} (open squares), and R_P (open circles) for sample *B* at T=7 K and V_{bias}=10 mV. MR oscillations between 2% and 3.5% are observed as a function of gate voltage, mostly due to oscillations in R_{AP}. (b) A subsequent gate voltage scan with finer steps was performed under the same conditions, and matching MR oscillations were observed.

only those with nonlinear *I*-*V* curves have shown substantial MR. These data suggest that the MR can be enhanced by tunnel barrier engineering.

We investigated the gate voltage dependence of the MR by utilizing the degenerately doped Si substrate as a back gate that is isolated from the MG by 300 nm of SiO_2 [Fig. 1(c)]. For sample *B*, the gate voltage dependence of the MR, the resistance for the antiparallel magnetization state (R_{AP}), and the resistance for the parallel magnetization state (R_P) are shown in Fig. 4(a). The electric field effect on the resistance is rather weak, with changes in R_P less than 1% over the gate voltage range of −15 to 15 V. On the other hand, the MR exhibits oscillations between 2% and 3.5%, with most of this effect due to oscillations in R_{AP}. To confirm this behavior, a second scan with finer gate voltage steps was performed and matching oscillations were observed [Fig. 4(b)]. While gate-dependent MR oscillations in carbon nanotube spin valves are attributed to quantum interference effects,[5,16,17] in our case further systematic studies are needed to understand the physical origin of the oscillatory behavior.

Finally, we note that we have fabricated and measured few-layer graphene (FLG) spin valves with FLG thickness as low as 1 nm (as determined by AFM), but we have not observed MR in these devices. One of the possible causes for the lack of MR in FLG spin valves could be due to the preparation of graphite flakes by sonication, which may introduce defects or ripples in thinner flakes. Alternative approaches to graphene fabrication are now under way.

In conclusion, magnetoresistance measurements provide strong evidence for spin-polarized transport in MG. We find that MgO tunnel barriers facilitate spin injection, and the bias dependence of MR is correlated with the nonlinear *I*-*V* characteristics. Oscillations in MR as a function of gate voltage are also observed.

The authors thank Ward P. Beyermann for technical assistance. This work was supported by ONR (Grant No. N00014-05-1-0568), the CNID program (Grant No. DOD/DMEA-H94003-06-2-0608), NSF (Grant No. DMR-0450037), and the Research Corporation.

*roland.kawakami@ucr.edu

[1] S. A. Wolf, D. D. Awschalom, R. A. Buhrman, J. M. Daughton, S. von Molnár, M. L. Roukes, A. Y. Chtchelkanova, and D. M. Treger, Science **294**, 1488 (2001).
[2] J. S. Moodera, J. Nassar, and G. Mathon, Annu. Rev. Mater. Sci. **29**, 381 (1999).
[3] K. Tsukagoshi, B. W. Alphenaar, and H. Ago, Nature (London) **401**, 572 (1999).
[4] L. E. Hueso, J. M. Pruneda, V. Ferrari, G. Burnell, J. P. Valdés-Herrera, B. D. Simons, P. B. Littlewood, E. Artacho, A. Fert, and N. D. Mathur, Nature (London) **445**, 410 (2007).
[5] S. Sahoo, T. Kontos, J. Furer, C. Hoffmann, M. Gräber, A. Cottet, and C. Schönenberger, Nat. Phys. **1**, 99 (2005).
[6] K. S. Novoselov, A. K. Geim, S. V. Morozov, D. Jiang, Y. Zhang, I. V. Grigorieva, S. V. Dubonos, and A. A. Firsov, Science **306**, 666 (2004).
[7] K. S. Novoselov, A. K. Geim, S. V. Morozov, D. Jiang, M. I. Katsnelson, I. V. Grigorieva, S. V. Dubonos, and A. A. Firsov, Nature (London) **438**, 197 (2005).
[8] Y. Zhang, Y. Tan, H. L. Stormer, and P. Kim, Nature (London) **438**, 201 (2005).
[9] Y.-W. Son, M. L. Cohen, and S. G. Louie, Nature (London) **444**, 347 (2006).
[10] S. Okada and A. Oshiyama, Phys. Rev. Lett. **87**, 146803 (2001).
[11] C. L. Kane and E. J. Mele, Phys. Rev. Lett. **95**, 226801 (2005).
[12] N. A. Sinitsyn, J. E. Hill, H. Min, J. Sinova, and A. H. MacDonald, Phys. Rev. Lett. **97**, 106804 (2006).
[13] E. W. Hill, A. K. Geim, K. Novoselov, F. Schedin, and P. Black, IEEE Trans. Magn. **42**, 2694 (2006).
[14] A. Fert and H. Jaffrès, Phys. Rev. B **64**, 184420 (2001).
[15] E. I. Rashba, Phys. Rev. B **62**, R16267 (2000).
[16] Th. Schäpers, J. Nitta, H. B. Heersche, and H. Takayanagi, Phys. Rev. B **64**, 125314 (2001).
[17] H. T. Man, I. J. W. Wever, and A. F. Morpurgo, Phys. Rev. B **73**, 241401(R) (2006).
[18] J. S. Bunch, Y. Yaish, M. Brink, K. Bolotin, and P. L. McEuen, Nano Lett. **5**, 287 (2005).
[19] R. Meservey and P. M. Tedrow, Phys. Rep. **238**, 173 (1994).
[20] M. Julliere, Phys. Lett. **54A**, 225 (1975).
[21] K. D. Belashchenko, E. Y. Tsymbal, M. van Schilfgaarde, D. A. Stewart, I. I. Oleinik, and S. S. Jaswal, Phys. Rev. B **69**, 174408 (2004).
[22] R. Thamankar, S. Niyogi, B. Y. Yoo, Y. W. Rheem, N. V. Myung, R. C. Haddon, and R. K. Kawakami, Appl. Phys. Lett. **89**, 033119 (2006).
[23] B. Nagabhirava, T. Bansal, G. U. Sumanasekera, B. W. Alphenaar, and L. Liu, Appl. Phys. Lett. **88**, 023503 (2006).
[24] G. Schmidt, D. Ferrand, L. W. Molenkamp, A. T. Filip, and B. J. van Wees, Phys. Rev. B **62**, R4790 (2000).
[25] X. Jiang, R. Wang, R. M. Shelby, R. M. Macfarlane, S. R. Bank, J. S. Harris, and S. S. P. Parkin, Phys. Rev. Lett. **94**, 056601 (2005).
[26] I. L. Spain, Chem. Phys. Carbon **16**, 119 (1981).
[27] G. K. White and S. B. Woods, Philos. Trans. R. Soc. London, Ser. A **251**, 273 (1959).
[28] Y. Lu, X. W. Li, G. Xiao, R. A. Altman, W. J. Gallagher, A. Marley, K. Roche, and S. Parkin, J. Appl. Phys. **83**, 6515 (1998).